2014 IEEE International Conference on Robotics & Automation (ICRA)
Hong Kong Convention and Exhibition Center
May 31 - June 7, 2014. Hong Kong, China

Energy Harvesting Analysis for *Moball*, A Self-Propelled Mobile Sensor Platform Capable of Long Duration Operation in Harsh Terrains

Matthew R. Burkhardt, Faranak Davoodi, Joel W. Burdick, Farhooman Davoudi

Abstract— **This paper considers the design and optimization of an autonomous electromechanical control and energy scavenging system for the wind-propelled *Moball,* a spherical mobile sensor platform concept [1, 2]. This mechanism converts mechanical motion to electrical energy, and the same mechanism can function as an actuator to self-generate motion. Simulations of a simplified model on flat ground show that a $2m$ diameter *Moball* operating in typical Arctic conditions can generate $1.8 - 2.7$W of power continuously while being wind-propelled. We also demonstrate a simple motion control algorithm, showing that self-propulsion in windless conditions requires $1 - 1.5\,W$. Hence, using this mechanism, a *Moball* can self-generate sufficient energy for long duration missions involving self-propulsion, sensing, and communication in harsh, cold, windy climates (e.g., Polar regions on Earth, or the surface of Titan or Mars) where solar energy may be limited. Simulations with key design parameters are also used to draw general conclusions regarding optimal design for energy recovery. The addition of springs inside the generating mechanism greatly increases the range of wind speeds over which *Moball* can harvest energy.**

I. Introduction

There are a number of harsh, windy environments where *in situ* mobile sensor networks could provide valuable data to help answer outstanding questions in planetary science. On Earth, climate change is a subject of great current concern, and some of the most important aspects of this change occur in the polar regions. Perennial sea ice, which is thicker and older ice that is important to the stability of the Arctic's sea ice, has declined precipitously in this decade, being replaced by thinner and weaker seasonal ice [3, 4]. These changes can have repercussions not only on the Arctic environment and global climate, but may potentially have profound impacts on global transportation, resource development, marine operations, food production, and national security.

Since the polar regions strongly impact global climate, future climate predictions are only as good as the factors upon which the polar models are based. Certain parameters, such as the surface albedo of polar snow and ice, atmospheric anomalies (e.g., CO_2 and methane concentrations, etc.), wind forces and direction, temperature variations, and change in the distribution of cold and warm waters, have been isolated as key factors contributing to the sea ice meltdown and global climate effects [5]. However, current measurement systems lack the time-responsiveness, accuracy, and spatial coverage required to effectively quantify each contributing factor (as well as their seasonal variations) and to identify other missing factors. Information on these quantities is critical to improving seasonal-to-decadal prediction models across local, regional, and global scales for scientific research, as well as predictions of global climate change's impact on domains such as agriculture, shipping, and natural disasters.

Better models require large-scale measurements of temperature, pressure, wind speed, wind direction, snow depth, ice thickness, etc., as well as their variations in space and time, to be measured across the Arctic and Antarctic. Such measurements could be realized in many ways. Most previously launched or envisioned missions for monitoring the environmental characteristics of the Arctic/Antarctic are based on remote sensing systems. It is important to have "ground truth" measurements to verify and calibrate these measurement systems [6]. Moreover, many quantities of interest cannot be measured reliably, or at all, from remote sensing craft. A network of sensors could be distributed across different sectors and sea ice classes to maintain measurements in key areas and to avoid data gaps in time and space. Deploying a network based on fixed-location sensors across these vast regions would be prohibitively expensive. Mobile sensor platforms can potentially implement large scale coverage in an easier and more cost-effective approach.

Long-duration operation of mobile sensors is essential to meet the science needs of observations having seasonal or perennial duration in the Arctic/Antarctic. Autonomous and sustainable *in situ* sensor networks must also be able to transmit observations between themselves and remote communications assets. Hence, to prolong service life and science impact, a deployed sensor network must harvest sufficient energy from its environment to sustain communication, mobility, and sensing systems. Solar energy is not a reliable source in these polar regions, which experience several months of darkness annually.

Mars is another windy environment of scientific interest where a distributed mobile sensor network could enhance understanding of geology and climate. The solar-cell powered Spirit and Opportunity rovers had to cease operation in the Martian winter due to insufficient solar intensity, and some regions of Mars are quite dusty. Similarly, Saturn's moon Titan has a dense atmosphere with consistent wind at ground level, and very little sunlight reaching its surface due to atmospheric opacity.

In previous work [2, 7] Davoodi and co-workers have proposed to use a controllable and long lasting network of self-powered mobile sensor platforms, dubbed *Moballs* (see Section II for more details), to carry out distributed

* Matthew R. Burkhardt and Joel W. Burdick are with the Mechanical Engineering Department, California Institute of Technology, Pasadena CA 91125 USA (e-mail: mburkhar@caltech.edu).
Faranak Davoodi is with the Jet Propulsion Laboratory, California Inst. of Techn., Pasadena CA (e-mail:faranak.davoodi@jpl.nasa.gov).

measurements in such environments. Each *Moball* is equipped with an array of low-power and low-mass sensors and electronics. *Moballs* can communicate peer-to-peer with other *Moballs*, as well as with orbiters and other in-situ assets when in view. This creates a wireless mesh network and provides an interface for a global control system that will ensure desired area coverage, hazard avoidance, while optimizing *Moball's* exploring efforts according to available resources (power, memory, and bandwidth). Unlike previous wind-driven designs, *Moball* incorporates a novel combined mechanical control and energy scavenging system—essentially regenerative actuators. This system can steer the wind-driven vehicle to maintain coverage over a geographic area, or to precisely position a sensor for scientific measurements. Because the same mechanism can scavenge wind energy, *Moball* is capable of long-duration operation in the harsh polar climate. This paper considers and optimizes the design of the energy scavenging mechanical system, showing that in its' intended environments, enough energy can be extracted to support prolonged system operation.

Structure of the Paper. After reviewing prior work in the rest of this section, Section II introduces *Moball's* design, focusing on the energy harvesting system while Section III presents *Moball's* governing equations. Section IV describes simplified energy-harvesting simulations, and Section V presents a motion-generating controller and simulations of self-generated motion. Section VI provides a detailed discussion of the results to draw general conclusions about energy harvesting design principles for *Moball*.

Relation to Previous Work. Several previous works have considered mobile sensor platforms that can harvest energy, generate motion, and gather and transmit data. Liquid Robotics' *Wave-Glider* [8] is a submerged glider tethered to a floating buoy, which harnesses wave-energy to produce forward motion while using solar arrays to power on-board electronics. This configuration autonomously circumnavigated the Island of Hawaii in 2009. *Webb et al.* conceptualized and tested an underwater vehicle that propels itself by converting thermal gradients into buoyancy changes [9]. *Buckle et al.* demonstrated that thermal gradients along the ocean's depth could partially replenish the energy load imposed by sensors and actuation of an autonomous underwater vehicle [10]. *Erturk et al.* and *Secord et al.* utilized the forward and reverse-piezoelectric effect to generate thrust and harvest energy from hydrodynamic drag, although sensors were not employed in these designs [11, 12]. *Yu et al.* determined that endowing sensor nodes with mobility increased network lifetime when each of the nodes harvest energy and transmit data with finite on-board energy constraints [13]. To our knowledge, the wind-driven energy harvesting approach presented in this paper is new to the field of robotics.

Moball is not the first wind-driven mobile sensor module. The Jet Propulsion Laboratory's (JPL) *Tumbleweed* is a superficially similar concept, and has been proposed for use on Earth, Mars, Saturn's moon Titan, and Neptune's moon Triton [14-16]. *Tumbleweed* is "assumed to be a perfect, inelastic, homogeneous sphere that rolls without slip" and its' motion is passive and dictated by the wind, although there have been suggestions to implement control [17]. *Moball* augments these abilities with active trajectory control and energy harvesting, which increases network flexibility, productivity, and lifespan.

II. Background: Moball's Design

Moball is a spherical mobile sensor platform that combines mobility and energy harvesting to allow for autonomous data gathering and transmission over large terrains and time-spans. It can move via rolling, bouncing, saltation through the air, and skidding on ice.

Fig. 1 illustrates *Moball's* basic design. *Moball* is an inflatable sphere whose optimal diameter depends on the wind distribution of the intended environment (see Section V). *Moball's* inflate-upon-arrival capability facilitates ease of transportation to the region of interest. *Moball's* exterior is composed of abrasion-resistant fiber cladding and rugged polymer. For additional details regarding proposed *Moball* mission and communication systems architecture, sensing, deployment, and task planning, see [2, 7] This paper focuses solely on the potential for wind-driven energy harvesting with this design.

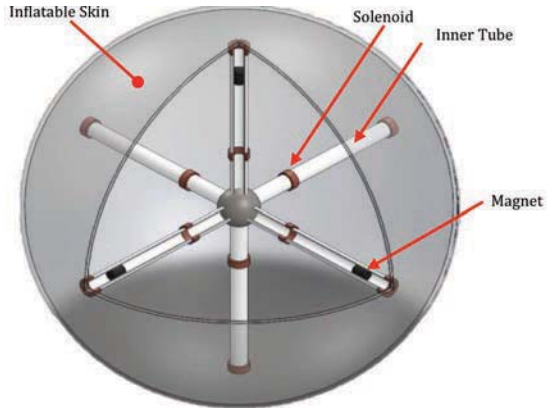

Figure 1: Simplified cutaway view of *Moball*. Sensory systems, battery, computation, and communication are not shown for clarity.

Moball's energy harvesting and self-propelled motion are intended to come from an electromechanical apparatus, depicted in *Fig. 1*. The mechanism consists of three orthogonal tubes that are rigidly fixed inside *Moball*. Concentric and cylindrical magnets lie inside each tube, and can slide freely as the ball moves under a wind force. Concentric and exterior to each tube are several solenoids. As the wind rotates *Moball*, the magnets pass through the solenoids and the resulting change in magnetic flux through the solenoid generates energy due to Faraday's Law of Induction. Harvested energy is stored in an on-board battery. The apparatus can also be operated in reverse. When current is passed through a solenoid, a nearby magnet experiences a force proportional to the applied current and the amount of magnetic coupling. By coordinating the solenoid currents, it is possible to move each of the magnets such that *Moball's* center of mass (COM) is shifted away from the center of rotation (COR). A non-collocated COM and COR will bias rolling, or generate rolling from standstill, and this is the basis for *Moball's* steering and self-propulsion.

III. Background: Governing Equations

This section develops simplified electromechanical and kinematic equations needed to assess *Moball's* energy harvesting capabilities. For simplicity, we analyze a planar version of the energy scavenging and motion control system. Note that for general *Moball* motions, at least one of the three axes can take advantage of *Moball's* rotation, and so the planar model should provide reasonable energy harvesting estimates.

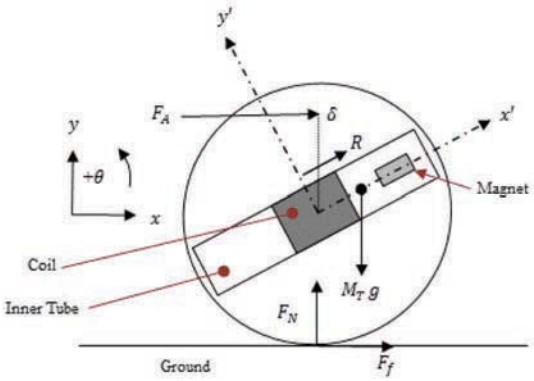

Figure 2: Coordinate frames used in *Moball's* dynamical equations of motion, as well as moments and forces applied to *Moball* rolling on a plane with no-slip.

A. Dynamic Equations

Fig. 2 depicts a 2-dimensional free-body-diagram, of the simplified *Moball* model. We assume *Moball* rolls without slip on a flat surface. Let (x, y) denote the coordinates of a fixed inertial frame, while locations in a body-fixed coordinate frame are described by (x', y'). The COM's acceleration with respect to the inertial frame is given by (1).

$$\vec{a}_{com} = \vec{a}_{cor} + \ddot{\vec{\theta}}\times\vec{R} + \dot{\vec{\theta}}\times\left(\dot{\vec{\theta}}\times\vec{R}\right) + 2\dot{\vec{\theta}}\times\dot{\vec{R}} + \ddot{\vec{R}} \quad (1)$$

The COR's acceleration with respect to the inertial frame is given by $\vec{a}_{cor}$ and the COM's position, velocity and acceleration with respect to the non-inertial frame are given by $\vec{R}$, $\dot{\vec{R}}$, and $\ddot{\vec{R}}$, respectively. *Fig.* 2 illustrates the forcing that is present on the rolling ball assuming planar rolling without slip. An applied force F_A, which models the driving wind force, acts at a distance δ from *Moball's* COR. In this preliminary analysis, the applied force is given by (2).

$$F_A = \frac{1}{2}C\rho A(V_w - V_{cor})^2 - \frac{1}{2}C\rho A V_{cor}^2 \quad (2)$$

The applied force is caused by a horizontal wind with velocity V_w and air density ρ, producing a driving force proportional to *Moball's* cross-sectional area A and drag coefficient C. V_{cor} represents *Moball's* horizontal velocity. The second term in (2) is the result of aerodynamic drag caused by *Moball's* motion through ambient air. The no-slip condition implies (3) and (4) and an application of Newton's Law along the horizontal as well as summing moments about the COR yields (5) and (6).

$$a_{y,cor} = 0 \quad (3)$$

$$a_{x,cor} = -R\ddot{\theta} \quad (4)$$

$$F_f + F_A = M_T a_{x,com} \quad (5)$$

$$(R^2\sin(\theta)\,M_T + I_{cor})\ddot{\theta} = F_f r - M_T g R cos(\theta) - F_A\delta \quad (6)$$

where F_f is the frictional force necessary to enforce the no-slip condition, which can be found using (1), (3), and (4). M_T and I_{COR} are *Moball's* total mass and moment of inertia about the COR, respectively. *Moball's* radius is given by r.

B. Electrodynamic Solenoid and Coupling Model

Applying Newton's Law to a magnet in the non-inertial frame yields (7). An electromagnetic drag force, F_{em}, opposes the magnet as it moves near the solenoid, according to Lenz's Law. The electromagnetic drag force between a solenoid and a dipole magnet is derived identically to that found in [18], and is detailed below for completeness.

$$\ddot{x}_m = \frac{F_{em}}{M_m} - gsin(\theta) + (\dot{\theta})^2 x_m \quad (7)$$

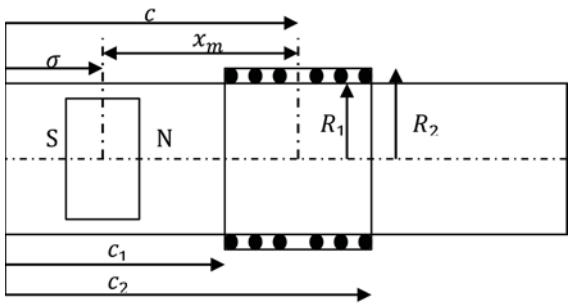

Figure 3: Important parameters used to derive electromagnetic drag force and power generation in a solenoid.

Fig. 3 depicts the important parameters used in this derivation. A dipole magnet approaches a single solenoid at a distance σ from one end of *Moball's* inner tube. According to Faraday's Law of Induction, a potential ε is induced in the coil given by (8). The induced voltage is proportional to the magnet's velocity through an undetermined coupling factor α, which is dependent on the magnet's position.

$$\varepsilon = \alpha(\sigma) * \dot{\sigma} \quad (8)$$

Assuming perfect energy conversion between the mechanical and electrical domains, an expression for F_{em} is given by (9), where I is the induced current. The coupling factor α can be solved analytically using Faraday's Law of Induction for an approaching magnet, given by (10). $\vec{B}$ is the magnetic flux density and the path integral is evaluated over the total length of wire, l_W, comprising the solenoid. If we choose to express the dipole's magnetic field in cylindrical coordinates, and note that $\vec{B}$ is invariant in the circumferential direction, evaluating (10) simplifies to (11).

$$F_{em} = \alpha(\sigma) * I \quad (9)$$

$$\varepsilon = \oint_{l_W}\left(\vec{\dot{x}}_m\times\vec{B}\right)\cdot d\vec{l} \quad (10)$$

$$\varepsilon = \oint_{l_W} -\dot{x}_m B_r\, dl \quad (11)$$

Further, using the relationship $c = \sigma + x_m$ from *Fig. 3* and substituting (8) into (11) results in a simple expression for $\alpha(\sigma)$ given by (12). To evaluate this integral, the solenoid is assumed to be tightly wound, such that the average of B_r over the total length of the solenoid's wire is approximately equal to the average of B_r over the solenoid's volume. This approximation is shown in (13) where the solenoid's volume is given by V_c.

$$\alpha(\sigma) = \oint_{l_W} B_r dl \tag{12}$$

$$\alpha(\sigma) = \left(\frac{1}{l_W}\oint_{l_W} B_r dl\right) * l_W \cong \left(\frac{1}{V_C}\iiint_{V_C} B_r dV\right) * l_W \tag{13}$$

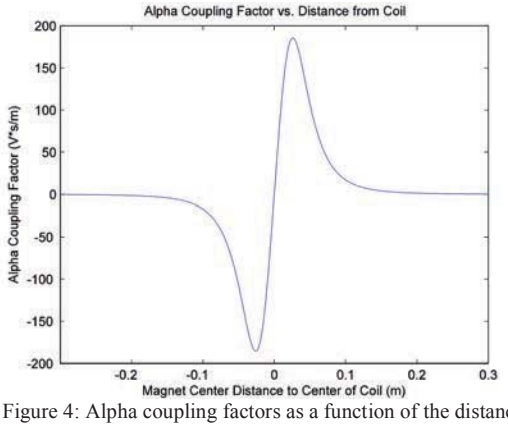

Figure 4: Alpha coupling factors as a function of the distance between the magnet and coil centers.

The radial component of the magnetic field for a cylindrical dipole magnet is available analytically, and can be used to solve the volume integral in (13) in closed form. For our purposes, $\alpha(\sigma)$ is more useful as a function of x_m so the variable substitution $c = \sigma + x_m$ is used to arrive at $\alpha(x_m)$, shown in *Fig. 4*.

It should be noted that although a no-slip condition was assumed in this work, more exotic behaviors such as bouncing and saltation can included by extending (1) to the horizontal and vertical directions.

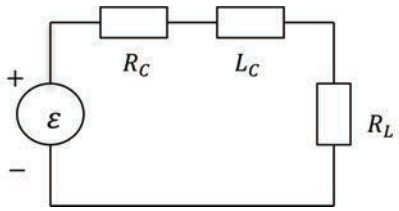

Figure 5: Equivalent circuit of solenoid

IV. Dynamic Simulations

The simulations presented in this section demonstrate how *Moball's* motion and energy generating performance are affected by key design parameters (an interpretation of these simulations can be found in Section V). Simulations were conducted using a single tube, a single dipole magnet, and n coils. These simulations do not take into account losses that might occur in circuit conductors or inefficiencies of battery charging. Each solenoid is assumed to be ideal and tightly wound. *Fig.* 5 illustrates the simple circuit model related to each coil. The induced voltage is serially connected to the coil resistance, R_c, the coil inductance, L_c, and a 100Ω resistor R_L. The governing circuit equation is given in (14), where I is the induced current.

$$-\varepsilon + IR_c + \frac{dI}{dt}L_c + IR_L = 0 \tag{14}$$

Equations (6)-(7) and n instances of (14) were solved simultaneously using MATLAB's *ode45* command. Power was measured across R_L and summed for each coil. Each simulation is initialized with *Moball* at rest, and the magnet stationary at the COR. Most quantities provided below are based on a 60 sec simulation, which fully captured transient and steady state behavior, with the majority of the time spent in steady state. The simulations were aimed at typical Arctic conditions, where the wind speed average is 4-6 m/sec.

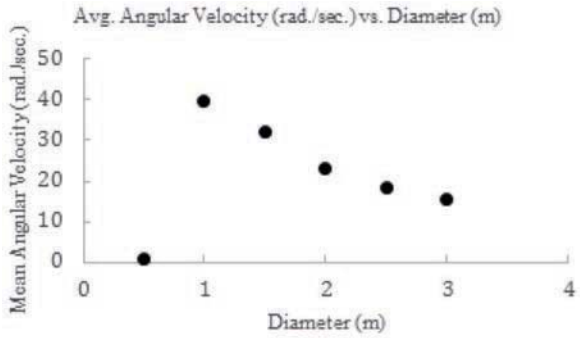

Figure 6: *Moball* diameter's effect on average angular velocity.

A. Effect of Diameter. *Fig.* 6 illustrates the effect that *Moball's* outer diameter has on its average angular velocity. A $5\ m/s$ wind was applied to a *Moball* with a constant mass of 12.585 kg and four coils equally and symmetrically spaced about the COR. *Moball's* inner tube increased with the diameter but its mass was held constant. Note, that since most of the simulation period was spent in steady state, *Moball's* actual mass did not greatly affect the results (figures in this section will be more fully discussed and interpreted in the next Section V).

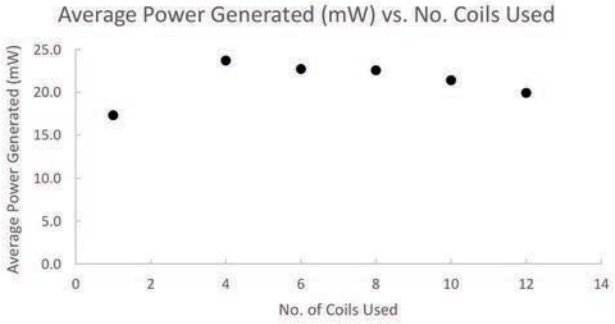

Figure 7: Power generation vs. number of coils.

B. Effect of Coil Parameters. *Fig.* 7 compares the average power generated as a function of the number of coils positioned equally and symmetrically along *Moball's* inner tube. A $5\ m/s$ wind was applied to a $2m$ diameter *Moball* of

constant mass. The total mass attributed to the coils was held constant and each coil was equally sized.

Fig. 8 demonstrates how the average power generated varies with the individual coil length. Again, a 5 m/s gust was applied to a *Moball* of constant mass. Four identical coils were spaced equally and symmetrically about the COR. The lengths of each individual coil was varied but the individual coil mass was held constant.

C. Energy Generation as a Function of Wind Speed, and impact of springs in the Linear Tube. *Fig.* 9 plots, in red, the average generated power as the applied wind speed varies from $3\,m/s$ to $6\,m/s$, in $0.2\,m/s$ increments for a *Moball* with a constant mass of $6.585\,kg$, $2m$ outer

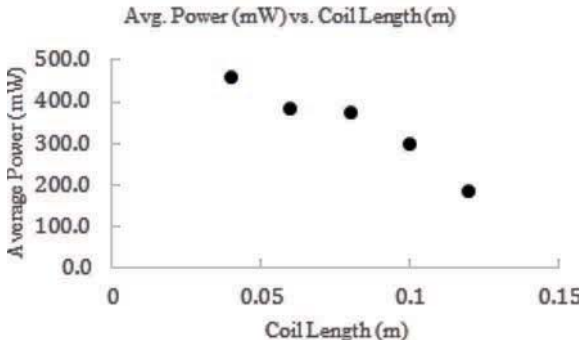

Figure 8: Effect of coil length on Average generated power

diameter, and four equally spaced $500g$ solenoid coils. Superimposed on *Fig. 9,* in black, is the average power generated when the *Moball* has linear springs inside its inner tube at the end-caps. Each spring has a relaxed length of $0.3\,m$ and a spring constant of $200\,N/m$. Four identical coils were centered at $x' = \pm 0.3m$ and $x' = \pm 0.75m$ to ensure that the magnet could pass through each coil.

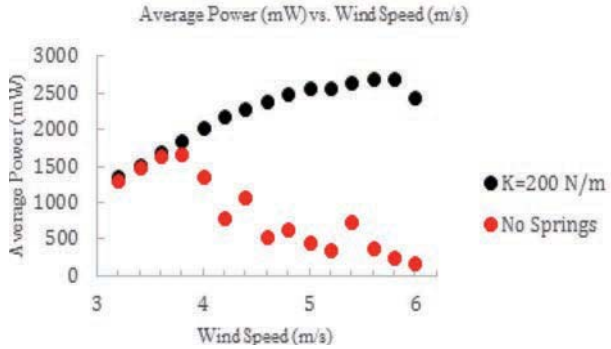

Figure 9: Average Power generated during 60 sec. interval vs. wind speed, for case of no springs (red) vs. springs (black).

V. Self-Propulsion & Power Consumption

A simple finite-state machine controller was developed to illustrate *Moball's* self-propulsion and to obtain a first-order approximation to the power required for propulsion on flat ground. Equation (15) governs the magnet's dynamics in the non-inertial frame, where F_a is an applied force arising from the current passed through coils nearby the magnet.

$$\ddot{x}_m = \frac{F_a}{M_m} - gsin(\theta) + (\dot{\theta})^2 x_m \tag{15}$$

The gravitational and centrifugal terms are taken to be time-varying disturbance forces and (15) is linearized about an equilibrium magnet position, x_{me}, and equilibrium magnet velocity, $\dot{x}_{me}$. The applied force necessary to sustain this equilibrium configuration is given by (16).

$$F_{ae} = M_m(gsin(\theta) - \dot{\theta}^2 x_{me}) \tag{16}$$

Equation (15) is then put into state-space form and full-state feedback is applied. Since (15) is 2nd order, controller constants K_1 and K_2 can be defined by specifying a damping ratio and settling time. A damping ratio of $\frac{1}{\sqrt{2}}$ and a settling time of $2s$ are selected. The applied force to move the magnet to a stationary position x_{me} is then given by (17)-(19).

$$F_a = -K_1(x_m - x_{me}) - K_2\dot{x}_m + M_m(gsin(\theta) - \dot{\theta}^2 x_{me}) \tag{17}$$

$$K_1 = M_m * \left(\left(\frac{4}{T_s\zeta}\right)^2 + \dot{\theta}^2\right) \tag{18}$$

$$K_2 = 8\frac{M_m}{T_s} \tag{19}$$

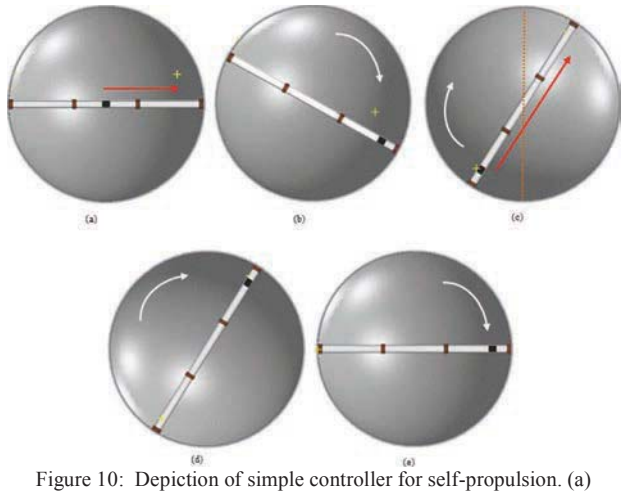
Figure 10: Depiction of simple controller for self-propulsion. (a) Magnet moves along the positive x' axis shown in yellow, (b) *Moball* rolls, (c) Magnet passes the vertical axis, and is moved in the negative x' direction, (d) Magnet is fixed and (e) *Moball* continues to roll. This process is repeated

To generate forward motion, the equilibrium position of the magnet, x_{me}, is changed depending on *Moball's* orientation. Initially, *Moball* is at rest and the magnet is commanded to move from the COR to the positive x' axis as shown in *Fig. 10*. A non-collocated COR and COM then cause *Moball* to rotate in the clockwise direction. Once the x' axis passes the vertical inertial axis, x_{me} is reflected to the negative x' axis. Again, a non-collocated COR and COM cause *Moball* to roll in the clockwise direction. This process is repeated to generate forward motion.

Simulations of $100s$ duration were conducted on *Moball* with four $500g$ coils equally and symmetrically spaced

about its COR. No wind propelled *Moball* during these simulations, but air drag was included. The electromagnetic drag force, F_{em}, was disabled in (7) since each coil propels the magnet instead of opposing it. The magnet's mass was adjusted from $400g$ to $800g$ in $25g$ increments. The magnet's length was held constant at $0.08m$ but its radius varied to accommodate its changing mass. The inner radius of *Moball's* inner tube and coils were adjusted to avoid collisions. Power was averaged over $100s$ by calculating $F \cdot \dot{x}_m$ resolved in the inertial frame. *Fig. 11* demonstrates how changing the magnet's mass effects the average power requirements for the controller described in (11)-(13). The

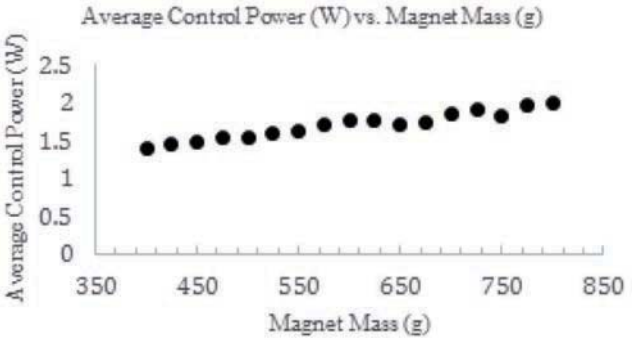

Figure 11: Average power needed to initiate motion vs. magnet mass.

equilibrium position, x_{me}, was chosen to be $\pm 0.85m$ in these simulations.

VI. Discussion of Design Principles

This section interprets the results of Section V and draws general conclusions about the key parameters affecting *Moball's* energy harvesting design.

Wind speed and Ball Diameter. *Fig.* 6 showed the effect of *Moball's* diameter on its' average angular velocity. For diameters $\ll 1m$, *Moball's* average angular velocity is negligible since it does not present enough cross-sectional area to the wind, and hence the wind force cannot consistently rotate *Moball* when its COM and COR are non-collocated. *Fig. 6* clearly shows that once the wind force is strong enough to propel *Moball,* the average angular velocity decreases as *Moball's* diameter increases, with its' mass held constant. If we consider the average steady state force $\bar{F}_A$ and ball velocity $\bar{V}_{COR}$, then expanding and rearranging (2) results in (20):

$$\frac{2\bar{F}_A}{C\rho A V_w} = V_w - 2\bar{V}_{COR} \tag{20}$$

Taking the limit as A increases to infinity, we find that the steady-state ball velocity tends towards $\frac{V_w}{2}$. The no-slip condition implies that as the ball's diameter increases, its mean angular velocity tends towards (21). In the context of Section V's simulations, the average angular velocity tends to $2.5\ \frac{rad}{s}$ as the diameter increases.

$$\left|\dot{\theta}_{AVG}\right| \to \frac{V_w}{2r} \tag{21}$$

This result has important design implications. As we can see from (7), the centrifugal forces applied to the magnet are proportional to $\dot{\theta}^2$, and energy harvesting may become impossible if this force is too large, which results in the magnet becoming pinned to *Moball's* outer edge. Thus, *Moball's* diameter must be chosen based on the expected wind speed, and must be sufficiently large so that centrifugal forces do not prevent energy harvesting (though the inclusion of springs can help mitigate this effect). Another key variable controlling the centrifugal force is the magnet's mass, M_m. Several simulations (figures not shown) demonstrated that a magnet of $550g - 600g$ consistently harvested energy in a $2m$ diameter ball with a nominal wind speed of $5\ \frac{m}{s}$, which is typical of Arctic conditions.

Coil Design. *Fig. 7* demonstrates how the number of coils placed along *Moball's* inner tube effects average power generated. In this simulation, the total mass of all coils was held constant at $8kg$ and the number of coils varied. Naively, one would think that power would increase proportionally to the number of coils. However, *Fig. 7* suggests that there are an optimum number of coils used, after which additional coils do not improve (and actually reduce) energy harvesting. This effect can be explained by recalling that electromagnetic drag forces slow the magnet's velocity, decreasing the amount of energy harvested in subsequent coils through which the magnet passes. Hence, too many coils reduces the amount of magnet speed, limiting effective energy production

Fig. 8 shows a strong correlation between the length of each individual coil and power generation. For a fixed 0.08m magnet height, a fixed inner coil radius of $0.0325m$, and constant individual coil volume, power generation increases as the coil length decreases. Similar behavior has been noted in [18] and can be explained by looking at the electromagnetic coupling developed in that reference.

The induced voltage between a solenoid and a dipole magnet is given by (11). The contour integral is dependent on the solenoid's geometry, and B_r is the radial component of the dipole magnetic field. Induced coil voltage depends on the *net* radial magnetic flux that flows through the solenoid's body. When the magnet's center is outside the coil body, B_r is entirely positive or negative throughout the coil. As the magnet's center enters the coil body, B_r is both positive and negative within the coil, and the integral in (11) decreases as a result. Therefore, the most power is generated when the magnet is only partially in the coil. Although a shorter coil will generate more energy, it will also slow the magnet's velocity due to a higher electromagnetic drag force. This may reduce energy generation and again, a balance exists between generating energy and maintaining consistent magnet velocity. A clear area for improvement is optimization of the magnetic field shape for energy harvesting and control. Halbach magnet arrays, exotic materials, and different magnet geometries may increase energy harvesting and control authority.

Springs can enhance and broaden the conditions of energy recovery. *Fig. 9* shows the average power generated

by *Moball* under $3-6$ m/s wind speeds. Without springs, *Moball* generated a maximum average power of $1.674W$ at a wind speed of 3.8 m/s. Wind speeds greater than a critical value (3.8 m/s in this simulation) are characterized by greater centrifugal forces on the moving magnet, which results in pinning of the magnet to *Moball's* outer diameter. Clearly the magnet cannot generate much power in this condition, explaining why the average generated power decreases rapidly to $174\ mW$ at a wind speed of 6 m/s. It is interesting to note that between wind speeds of 3.8 and $6\ m/s$, there appear to be two resonant peaks at 4.4 and 5.4 m/s. Practically, *Fig. 9* demonstrates that a spring-less *Moball* design has a narrow band between wind speeds of $3-4.4\ m/s$ where average power over $1W$ can be expected, but that power generation drops dramatically at high speeds.

Superimposed on *Fig. 9* is the average power response of the same *Moball* with linear springs placed in the solenoid tube's end caps, and its' four coils rearranged to allow the magnet to pass through each coil. Immediately, it is noticed that centrifugal forces do not begin to noticeably effect energy harvesting until $5.8\ m/s$, and an average power greater than $1W$ can be expected over the full range of $3-6\ m/s$ wind speeds. Furthermore, the power response is smoother and approximately proportional to wind speed, as compared to a spring-less *Moball*. The extended range of operation allows for maximum average power of $2.696\ W$ at a wind speed of $5.6\ m/s$, which is well within typical wind speeds seen in the Arctic.

Linear springs prevent the centrifugal forces from pinning magnets to *Moball's* outer edge. While springs may help generate power over a large range of wind speeds, it may be impractical to counteract spring forces during solenoid driven motion control of the magnet's position and velocity. Hence, the spring forces should toggle between active an inactive states depending upon the status of *Moball's* energy harvesting or motion control operations. Such toggling may be implemented via calibrated air springs, mechanical latches, or electromagnetic repulsion. The use of nonlinear spring-elements may also improve energy harvesting over a wide range of wind speeds. It should be noted that using spring-like elements to broaden the operating bandwidth of piezoelectric-based energy harvesting system is discussed in *Roundy et al.* [19].

Balancing Energy Harvesting with Motion Control. Practically, the best and most efficient control of magnet position and velocity using solenoids would arise from many small solenoids along the tube length, as a solenoid's ability to impart a force on a magnet tapers dramatically outside of the solenoid's body. Thus, many small solenoids along *Moball's* length would decrease the actuation energy necessary for control, but such a design may not be optimal for energy harvesting. Energy harvesting and actuation energy considerations must be optimally balanced when designing coil placement in a *Moball* prototype. Moreover, the balance between energy generation and control may be improved by dedicating a few large coils to energy harvesting and many smaller coils to control.

Factors which influence self-propulsion. *Figs.10* and *11* illustrate the operation of a simple controller to generate forward motion, and the average power required to drive magnets of varying mass to generate the motion. *Fig. 11* shows the intuitive result that larger mass magnets require greater power to control. However, magnets of greater mass command greater control authority. A $400g$ magnet and the described controller caused *Moball* to rotate with an average speed of $12.38\ RPM$, whereas a magnet of $800g$ caused *Moball* to rotate with an average speed of $16.42\ RPM$. Magnets with masses in between $400g$ and $800g$ generated average rolling speeds that monotonically increased.

Fig. 11 shows that the average power required to drive a $400g$ magnet is $1.388\ W$, while an $800g$ magnet required $1.989W$. It is interesting to note that for a $650g$ magnet the controller required less power than the $600g$ magnet but it generated a higher average rolling speed. A similar phenomenon occurred for the $750g$ magnet. These anomalies can be understood by *Fig. 10*c. For most values of magnet mass, the controller pushes the magnet to the other side of the x' axis, acting against gravity the entire duration. However, during the $650g$ and $750g$ simulations, *Moball* is rotating at a speed such that by the time the controller moves the magnet to the other side of the x' axis, gravity has little effect (since the x' axis is horizontal). This suggests that it may be possible to tune either *Moball's* or the controller's parameters to take advantage of resonance and achieve forward motion for significantly less power. Practically speaking, the required power suggested by these simulations is likely to be a significant over-estimate of the power needed to generate motion, as an optimal control algorithm should generate forward motion for even less power than what is reported here.

Overall Power Budget Summary. A $2m$ to $3m$ diameter *Moball* experiencing sustained winds between 4-6 m/sec (typical of the Arctic) is expected to harvest 1700-2800 mW, with realistic losses included. Rolling friction and the lack of perfect energy conversion between the electrical and mechanical domains are realities that will reduce the amount of energy harvested relative to our simulations. However, significant improvements in the design including multiple solenoid tubes, coil optimization, nonlinear spring-elements, and magnet optimization will recoup many of the losses.

Such power is more than ample to sustain full system operation during wind-driven motion. Peer-to-peer transceivers such as the *Libelium Waspmote* can transmit 10's of kilobits of data per second over a $7\ km$ distance for a $50mW$ power draw[20]. An onboard micro-controller can operate for a few hundred milliwatts. Further, a suite of low-power MEMS sensors measuring surface winds, temperature, pressure, humidity, and light intensity, can be operated at an energy cost of less than $50mW$ [21, 22]. Molecular detection sensors operate at a similar power level.

Thus, even with these system power draws, a *Moball* working in the Arctic can store enough electrical energy during its wind driven motion to power subsequent intervals of self-generated motion during windless conditions. With *Moball* beginning from rest, self-propulsion is expected to

draw an average of $1000mW$ to $1500mW$ for motion on flat ground, with losses included. A refinement that must be incorporated into the model is the relationship between the current passed through the coil and the resultant force acting on the magnet, incorporating losses between the electrical and mechanical domain. It is also expected that the rudimentary controller described in Section V could be optimized, resulting in more economical locomotion than what is reported in our simulations.

VII. Conclusion

Moball is a novel terrestrial sensor platform design that is capable of harvesting wind energy and generating locomotion through a single mechanism. The study presented in this paper demonstrated that a nontrivial amount of power can be generated by a $2-3\,m$ diameter *Moball* under sustained winds of 4 m/s to 6 m/s (which is typical of the Arctic). This power is ample to run *Moball's* onboard low-power sensing, computing, and communication system. Moreover, *Moball* can self-generate movement for useful distances (e.g., hundred meters) based on energy stored from previous wind-driven motion. While the simulations and analysis in this paper are highly idealized, they demonstrate the potential for long-duration operation of an autonomous wind-driven sensor platform in environments (e.g. Earth's polar regions, Mars, and Titan), where solar energy is either unavailable or insufficient for extended periods. Section VI also presented general design rules for energy harvesting in this class of systems.

Ongoing work seeks to optimize the energy harvesting capabilities through the use of novel magnet designs (e.g., Halbach arrays) and nonlinear spacing between coils. We also seek to minimize the power needed for self-motion generation through the use of optimal control methods.

Acknowledgments

This work was supported in part by a California Institute of Technology fellowship for the first author. The second author was partially supported from the Data Analysis group, Jet Propulsion Laboratory.

References

1. Davoodi, F., Davoudi, F., *Design for the Structure and the Mechanics of Moballs*. NASA Technical Briefs, October 2012. **36**(10): p. 66-68.
2. Davoodi, F., Hajimiri, A., Murphy, N., Mischna, N., Nesnas, I., Nikzad, S. *Gone with the Wind On Mars (GOWON): A Wind-Driven Networked System of Mobile Sensors on Mars*. in *Concepts and Approaches for Mars Exploration*. 2012.
3. Parkinson, C.L. and D.J. Cavalieri, *Arcti Sea Ice Variability and Trends, 1976-2006.* Geophys. Re. Lett., 2008. **3**(11).
4. Nghiem, S.V., I.G. Rigor, D.K. Perovich, P. Clemente-Colon, J.W. Weatherly, and G. Neuman, *Rapid Reduction of Arctic Perennial Sea Ice.* Geophys. Res. Lett., 2007. **4**(L19504).
5. Dery, S.J. and M.K. Yau, *Large-scale mass balance effects of blowing snow and surface sublimitation.* J. Geophy. Res., 2002. **107(D3)**(4679).
6. Burgess, E.W., R.R. Forster, J.E. Box, E. Mosley-Thompson, D.H. Bromwich, R.C. Bales, and L.C. Smith, *A Spatially Calibrated Model of Annual Accumulation Rate on the Greenland Ice Sheet (1958-2007).* J. Geophy. Res., 2010. **115**(F02004).
7. Davoodi, F. and N. Murphy *Wind-Driven Wireless Networked System of Mobile Sensors for Mars Exploration*. Nasa Tech Briefs, January, 2013. 25-26.
8. Hine, R., S. Willcox, G. Hine, and T. Richardson. *The Wave Glider: A Wave-Powered autonomous marine vehicle*. in *OCEANS 2009, MTS/IEEE Biloxi - Marine Technology for Our Future: Global and Local Challenges*. 2009.
9. Webb, D.C., P.J. Simonetti, and C.P. Jones, *SLOCUM: an underwater glider propelled by environmental energy.* Oceanic Engineering, IEEE Journal of, 2001. **26**(4): p. 447-452.
10. Buckle, J.R., A. Knox, J. Siviter, and A. Montecucco, *Autonomous Underwater Vehicle Thermoelectric Power Generation.* Journal of Electronic Materials, 2013. **42**(7): p. 2214-2220.
11. Erturk, A. and G. Delporte, *Underwater thrust and power generation using flexible piezoelectric composites: an experimental investigation toward self-powered swimmer-sensor platforms.* Smart Materials & Structures, 2011. **20**(12).
12. Secord, T.W., A. Mazumdar, and H.H. Asada. *A multi-cell piezoelectric device for tunable resonance actuation and energy harvesting*. in *Robotics and Automation (ICRA), 2010 IEEE International Conference on*. 2010.
13. Shengwei, Y. and C.S.G. Lee. *Lifetime maximization in mobile sensor networks with energy harvesting*. in *Robotics and Automation (ICRA), 2011 IEEE International Conference on*. 2011.
14. Southard, L., T.M. Hoeg, D.W. Palmer, J. Antol, R.M. Kolacinski, and R.D. Quinn. *Exploring Mars Using a Group of Tumbleweed Rovers*. in *Robotics and Automation, 2007 IEEE International Conference on*. 2007.
15. Jones, J.A., *Inflatable Vehicles for In-Situ Exploration of Titan, Triton, Uranus, Neptune*, in *Forum on Innovative Approaches to Outer Planetary Exploration 2001-2020*. 2001.
16. Behar, A., F. Carsey, J. Matthews, and J. Jones. *An antarctic deployment of the NASA/JPL tumbleweed polar rover*. in *Automation Congress, 2004. Proceedings. World*. 2004.
17. Antol, J., P. Calhoun, J. Flick, and G. Hajos, *Low cost Mars Surface Exploration: The Mars Tumbleweed.* Nasa Tech Briefs, 2003: p. TM-2003-212411.
18. Joyce, B.S., *Development of an Electromagnetic Energy Harvester for Monitoring Wind Turbine Blades*, in *Mechanical Engineering*. 2011, Virginia Polytechnic Institute and State University: Blacksburg, Virginia.
19. Roundy, S.J. and J. Tola. *An energy harvester for rotating environments using offset pendulum dynamics*. in *Solid-State Sensors, Actuators and Microsystems (TRANSDUCERS & EUROSENSORS XXVII), 2013 Transducers & Eurosensors XXVII: The 17th International Conference on*. 2013.
20. *Libelium Wireless Interfaces Technical Overview*. 2013 September 11th, 2013]; Available from: http://www.libelium.com/products/waspmote/interfaces/.
21. Sadeghi, M.M., R.L. Peterson, and K. Najafi, *Hair-based sensors for micro-autonomous systems*, in *Micro- and Nanotechnology Sensors, Systems, and Applications Iv*, T. George, M.S. Islam, and A. Dutta, Editors. 2012.
22. *Libelium Sensor Boards Technical Overview*. 2013 September 11th, 2013]; Available from: http://www.libelium.com/products/waspmote/sensors/.